The Astronomical Journal, 130:2241–2251, 2005 November

PUSHING THE LIMITS OF GROUND-BASED PHOTOMETRIC PRECISION: SUBMILLIMAGNITUDE TIME-SERIES PHOTOMETRY OF THE OPEN CLUSTER NGC 6791

J. D. Hartman, K. Z. Stanek, B. S. Gaudi, M. J. Holman, and B. A. McLeod
Harvard-Smithsonian Center for Astrophysics, 60 Garden Street, Cambridge, MA 02138; jhartman@cfa.harvard.edu, kstanek@cfa.harvard.edu, sgaudi@cfa.harvard.edu, mholman@cfa.harvard.edu, bmcleod@cfa.harvard.edu
Received 2005 April 21; accepted 2005 June 25

ABSTRACT

We present the results from a three-night, time-series study of the open cluster NGC 6791 using the Megacam wide-field mosaic CCD camera on the 6.5 m MMT telescope. The aim of this study was to demonstrate the ability to obtain very high precision photometry for a large number of stars. We achieved better than 1% precision for more than 8000 stars with $14.3 < R < 20.1$ and submillimagnitude (as low as 0.36 mmag) precision for over 300 stars with $14.6 < R < 16.3$ in the field of this cluster. We also discovered 10 new variable stars, including a possible δ Scuti variable with an amplitude of 2%, eight likely W UMa contact binaries, and a possible RS CVn star, and we identified seven suspected low-amplitude variables, including one star with an amplitude of 4 mmag. We comment on the implications of this study for a ground-based survey for transiting planets as small as Neptune.

Key words: binaries: eclipsing — δ Scuti — stars: variables: other — techniques: photometric

Online material: color figures

1. INTRODUCTION

Since the advent of high-quality CCDs there has been a great deal of effort to obtain high-precision (millimagnitude, or less than 1%) time-series, optical and infrared photometry for large numbers of stars. Photometry at the millimagnitude level of precision is considered a prerequisite in searches for transiting Jupiter-sized planets around solar-type stars. As a result, the number of groups that have achieved this level of precision is too many to list here (see, e.g., Horne [2003] for a list of transiting planet searches). The search for transiting planets has not been in vain; at the time of writing there are seven known transiting planets, six of which were first identified photometrically (Udalski et al. 2002a, 2002b, 2002c, 2003; Konacki et al. 2003, 2004, 2005; Bouchy et al. 2004; Pont et al. 2004; Alonso et al. 2004). Millimagnitude photometry has also contributed to the study of stars near the hydrogen fusion limit (Pont et al. 2005) and enabled the study of stellar variability with amplitudes of a few percent (e.g., Bruntt et al. 2003). With the number of transit surveys growing steadily, millimagnitude photometry has become routine. Pushing below 0.1%, however, has proven difficult.

To our knowledge, Gilliland et al. (1993) hold the record for the most precise (per exposure) ground-based photometry that has been reported. They achieved a precision as good as 0.25 mmag per exposure for a group of 12 stars in M67 that they monitored for solar-like oscillations. Prior to that, Gilliland & Brown (1992) achieved a precision of 0.75 mmag per exposure. In both of these cases only a handful of bright isolated stars were monitored. Since these projects were aimed at searching for short-timescale, solar-like oscillations, the authors applied high-pass filters to their light curves, thereby removing any long-timescale systematic trends together with any long-timescale variability. Ground-based, submillimagnitude per exposure photometry has also been obtained for individual bright objects (e.g., Jha et al. [2000], who obtained an rms of 0.8 mmag for the transiting system HD 209458 using a photometer; also see Kurtz et al. [2005]). Other attempts to achieve submillimagnitude precision from the ground have succeeded by time binning multiple millimagnitude-level exposures (e.g., Everett & Howell 2001).

Despite the difficulties in performing submillimagnitude photometry from the ground for large numbers of stars, the possible science rewards are compelling. Improving the precision of transit surveys by a factor of 10 would allow for the detection of 0.1% transits by Neptune-sized planets orbiting solar-type stars. It would also allow the exploration of a new regime of stellar variability.

As discussed in § 2, the Megacam instrument on the MMT[1] telescope is an ideal setup for achieving submillimagnitude photometry from the ground. By using CCDs with deep potential wells and superb sampling of the point-spread function (PSF) it is possible to collect enough photons from a star prior to saturation that the photon limit on the noise is well below 1 mmag. Using this camera we can achieve high-precision photometry without having to defocus the images (and thus increase the sky noise for the fainter stars) or implement special electronics to modify the shape of the PSF (see Tonry et al. [2005], who achieve high-precision photometry over a wide dynamic range by using an orthogonal-transfer CCD).

Motivated by the possibility of opening a new regime to ground-based, time-series campaigns, we set out to demonstrate photometry for a large number of stars with a per exposure precision as good as a few parts in 10,000 by conducting a short time-series study of the open cluster NGC 6791 using MMT and Megacam.

In § 2 we describe our observations. We follow with a discussion of our data reduction steps in § 3; in § 4 we describe the photometric precision we have achieved; in § 5 we present new variable stars that we have found in this field; and we finish with a discussion of our results, including the possibility of a search for transiting Neptune-sized planets in § 6.

2. OBSERVATIONS

The data for this project were obtained on the nights of 2004 October 4, 9, and 20 using the Megacam CCD mosaic (McLeod et al. 2000) mounted on the MMT 6.5 m telescope. The Megacam

[1] Observations reported here were obtained at the MMT Observatory, a joint facility of the Smithsonian Institution and the University of Arizona.

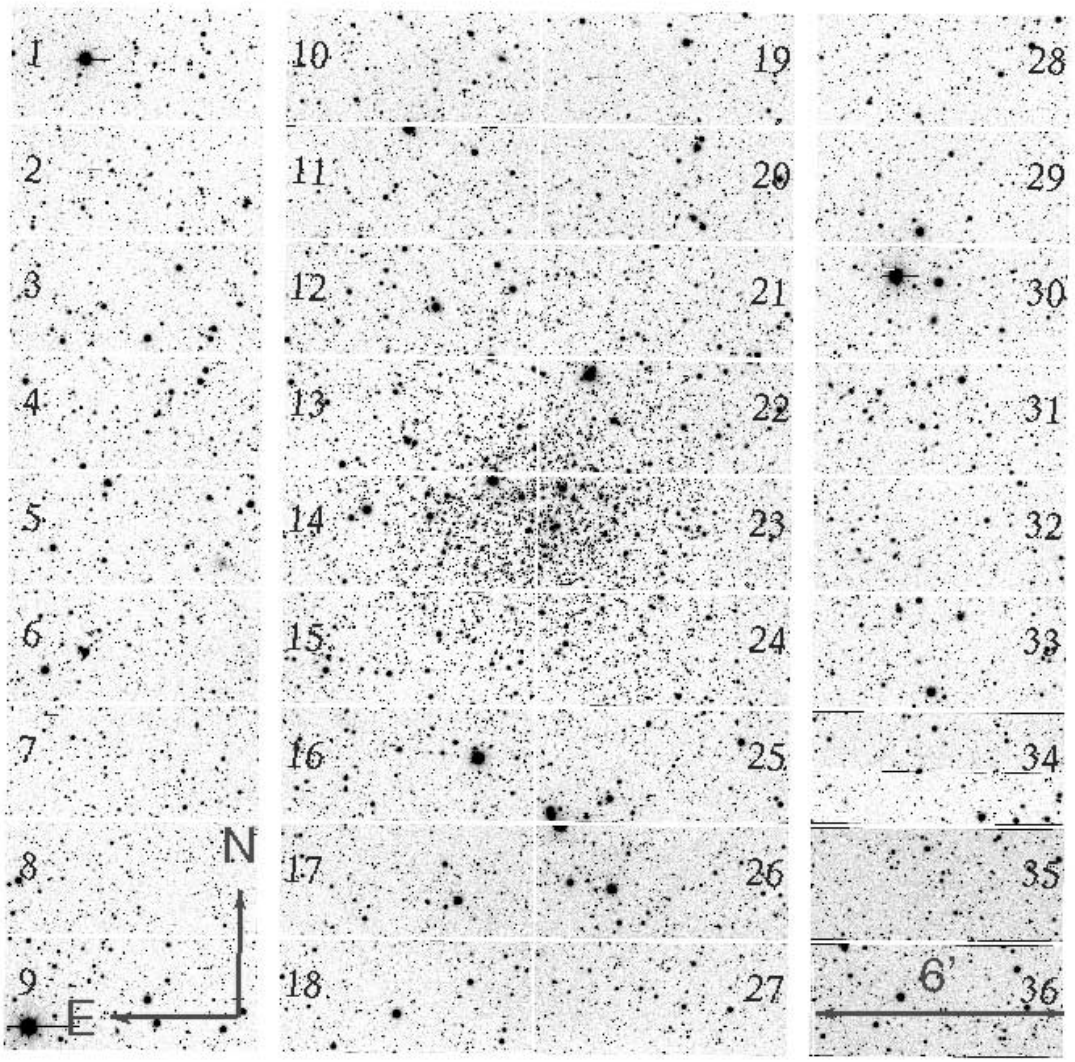

FIG. 1.—Megacam mosaic image of the open cluster NGC 6791. Chip labels are for reference in the text. [*See the electronic edition of the Journal for a color version of this figure.*]

instrument is a $24' \times 24'$ mosaic consisting of 36 2k × 4k, thinned, backside-illuminated CCDs that are each read out by two amplifiers. The mosaic has a pixel scale of 0.″08, which allows for a well-sampled PSF even under the best seeing conditions. The result is that in 1″ seeing one can collect as many as 2×10^7 photons from a single star prior to saturation, setting the photon limit for the precision in a single exposure at 0.25 mmag.

For this study we chose to observe the open cluster NGC 6791. This cluster has been studied extensively for variability by the PISCES project (Mochejska et al. 2002, 2005; additional variability surveys of this cluster include those by Kaluzny & Ruciński 1993, Ruciński et al. 1996, Mochejska et al. 2003, and Bruntt et al. 2003). As noted in Mochejska et al. (2005), the cluster is populous (Kaluzny & Udalski 1992), old ($\tau = 8$ Gyr), metal-rich ([Fe/H] = +0.4), and located at a distance modulus of $(m - M)_V = 13.42$ (Chaboyer et al. 1999).

We obtained 71 exposures centered on the cluster $(\alpha, \delta) = (19^{\rm h}20^{\rm m}53^{\rm s}.0, +37^\circ46'30''.0)$ (J2000.0) using a Sloan r' filter. Of these exposures, 20 were obtained on 2004 October 4 with a 2 minute exposure time, 17 on 2004 October 9 with a 2 minute exposure time, and 36 on 2004 October 20 with a 1 minute exposure time. The data on the first two nights were obtained with a gain setting of 10 e^- ADU^{-1}; after noting the possibility of nonlinearity in pixels with more than 2×10^5 e^- we switched to a gain of 3.5 e^- ADU^{-1} for the last night. In both cases we were not limited by the analog-to-digital converter. All images were read out using 2 × 2 binning (yielding a pixel scale of 0.″16), but this did not limit the number of electrons in the detector. For reference, we present a Megacam mosaic image of the field in Figure 1.

For the first night the seeing was highly variable, ranging from 1″ to 3″. On the second and third nights the seeing was relatively stable, but not exceptional, and ranged from 1″ to as high as 2″ in a handful of images. The poor conditions on the first night make the data unusable for precision photometry using our reduction techniques, although we include data from this night in the light curves presented in § 5.

3. DATA REDUCTION

The preliminary CCD reductions, including overscan, zero-level correction, and flat-fielding were performed using the standard routines in the IRAF MSCRED package.[2] We constructed a

[2] IRAF is distributed by the National Optical Astronomy Observatory, which is operated by the Association of Universities for Research in Astronomy, Inc., under agreement with the National Science Foundation.

master twilight flat field from 5, 19, and 5 individual twilight flat-field exposures for 2004 October 4, 9, and 20, respectively.

To obtain photometry we used the image subtraction methods from Alard & Lupton (1998; see also Alard 2000) as implemented in the ISIS 2.1 package.[3] The procedure we followed is similar to that described in, e.g., Hartman et al. (2004); here we only highlight differences from the procedure discussed there. The basic scheme is to match the PSF and background of a reference image to another image, subtract them, and perform photometry on the subtracted image. The photometry routine that comes with the ISIS package convolves a PSF determined empirically on the reference image, with the convolution kernel used to match the images, and then performs fixed-position, PSF-fitting photometry on the subtracted image.

We performed subtraction independently for 33 of the 36 CCDs in the mosaic (the three chips labeled 34–36 in Fig. 1 had artifacts that rendered them unusable at the time), dividing each CCD into two independent subregions. We created saturation masks for each image so that pixels above 60,000 ADU would not be used in the photometry extraction routines. Prior to registering the images we binned them 3×3. This reduced the FWHM of the PSF to 2–3 pixels over the range of seeings that were encountered and thus allowed us to use the existing ISIS routines without substantial modification. Reference images for each chip were created from the best seeing images on the third night.

Because one only measures differential flux with image subtraction, it is necessary to obtain base fluxes for the stars via another technique if one wishes to obtain light curves in magnitudes. We obtained these fluxes by performing PSF photometry on the reference images for each chip using DAOPHOT and ALLSTAR (Stetson 1987, 1992). To ensure that the fluxes that we measured in ISIS are on the same scale as those measured with DAOPHOT and ALLSTAR, we performed an aperture correction by measuring the flux on the reference images using aperture photometry with a radius equal to that used in ISIS and adjusting the PSF photometry to remove any systematic differences from the aperture photometry. The corrections were typically less than 0.1 mag (in absolute value), and all had an rms uncertainty less than 10 mmag. As a result, any systematic error in the amplitudes should be less than 1% of the stated amplitude.

We proceeded to obtain photometry for 27,885 stars on 33 CCDs with $13.9 < R < 24.0$. We calibrated the photometry to the R band using data provided to us from PISCES (B. Mochejska 2005, private communication).

Having obtained the light curves, we performed three cleaning steps. The first step was to remove any systematic changes in the zero points of the light curves. We did this by solving for the corrections to the zero points that minimize

$$\sum_{i,j} \frac{\left(m_{ij} + \Delta z_i - \bar{m}_j\right)^2}{\sigma_{ij}^2}, \tag{1}$$

where m_{ij} is the magnitude of the jth star at time i, $\bar{m}_j$ is the average magnitude of the jth star, σ_{ij} is the uncertainty in the magnitude of the jth star at time i and is calculated assuming photon noise and the gain listed in the Megacam Observers Manual, and Δz_i is the correction to the zero point at time i. The zero-point corrections were all less than 1 mmag and hence only affected the precision of the brightest stars.

In the second step we rejected observations, for each chip, for which a substantial percentage of stars on the chip (more than 4.5%) showed a greater than 3 σ deviation from their mean. This removed 3 or 4 of the 36 observations on the third night for most of the chips. The rejected observations were among the poorest seeing images for the night. For the second night we used a less stringent criterion of 19% to remove 1 or 2 of the 17 observations for most of the chips. We required a less stringent criterion because a greater fraction of the stars for which we extracted photometry were saturated in the longer exposures of the second night.

In the third step we implemented the cleaning algorithm presented by Tamuz et al. (2005, hereafter TMZ05). This algorithm is a more general version of the method described in the first cleaning step. The scheme is to minimize the expression

$$\sum_{i,j} \frac{\left(m_{ij} + a_i c_j - \bar{m}_j\right)^2}{\sigma_{ij}^2}, \tag{2}$$

where we now allow for epoch-dependent parameters (a_i) and star-dependent parameters (c_j). One identifies a number of possible sources for systematic trends in the data (e.g., trends dependent on the air mass or the linear position of the star) and then evaluates the initial relevant star (e.g., position) or epoch (e.g., air mass) parameters. The conjugate epoch parameters are then given by

$$a_i = \frac{\sum_j \left(m_{ij} - \bar{m}_j\right) c_j / \sigma_{ij}^2}{\sum_j c_j^2 / \sigma_{ij}^2}, \tag{3}$$

with a similar expression for the star parameters. Given this initial guess for the a_i and c_j, TMZ05 suggest iterating between solving for the a_i and the c_j to minimize equation (2). The resulting a_i and c_j are general parameters describing linear trends in the data that may not be related to the suspected trends used in generating the initial guess. In practice we found that the iterative procedure did not converge and instead used the Polak-Ribiere variant of the Fletcher-Reeves algorithm (Press et al. 1992) to minimize equation (2). To prevent large-amplitude variable stars from defining the linear trends we employed a simple σ clipping, requiring $|m_{ij} - \bar{m}_j| < 3\sigma_{ij}$ in evaluating equation (2). Using this algorithm we attempted to remove seven linear trends in succession: trends dependent linearly and quadratically on the air mass, linearly and quadratically on the x- and y-positions of the star on the CCD, and linearly on the phase of the moon [$\sin(\omega_m t)$, where ω_m is the angular frequency of the lunar phase]. We discuss the impact of this cleaning step on the photometric precision in § 4 and on the light curves of candidate variable stars in § 5.

Even with the aperture correction it is still possible for there to be a systematic error in the amplitudes of variations. This would happen, for example, if there was a systematic error in the ISIS photometry that might result from errors in the subtraction process. To ensure that we are not underestimating the amplitudes of our light curves, and hence overestimating our precision, we extracted photometry for a handful of simulated variable stars.

To add the simulated variable stars we first identified a bright isolated star on one of the images and extracted a small box around the star in every image. We then measured and subtracted the sky from the box, multiplied the box by a scaling factor, and added the result to another location on the image. In this way we simulated two variables stars with semiamplitude flux variations of 10% and 1%. We present the resulting light curves in Figure 2. The purpose of this procedure was to test for systematic errors in the amplitudes; we stress that the overall noise in the light curves

[3] The ISIS package is available from C. Alard's Web site at http://www2.iap.fr/users/alard/package.html.

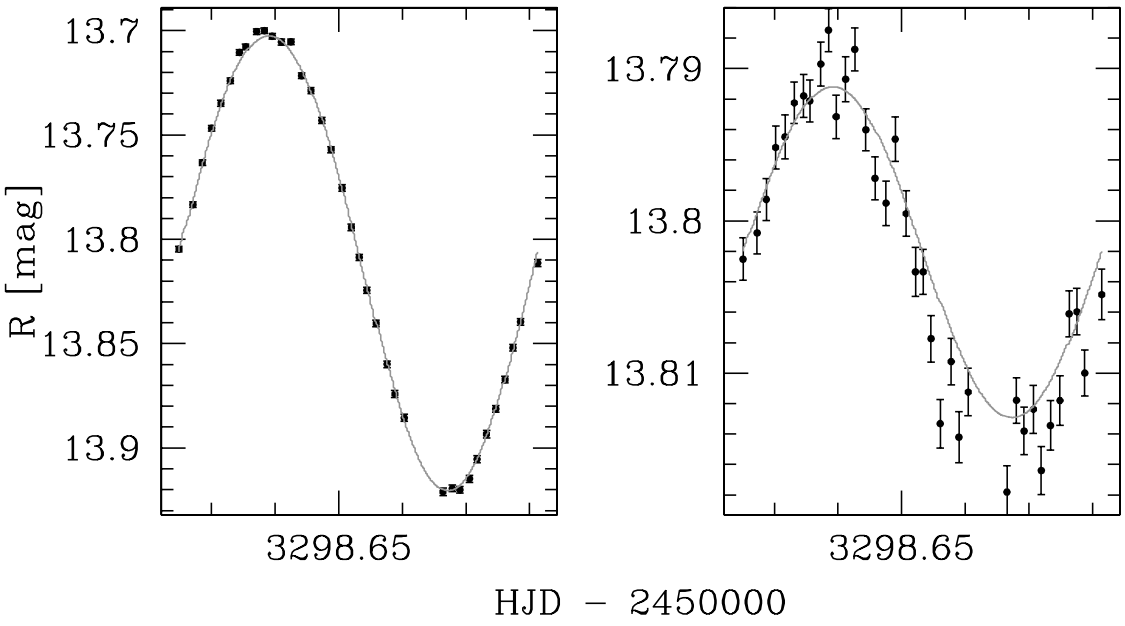

FIG. 2.—Light curves of simulated variable stars. Points were extracted using image subtraction; the solid line shows the input variable star signal. The noise in the light curve comes from the base star that is multiplied by the signal, as well as from errors in the simulation process. *Left*: A 10% semiamplitude variation; *right*: a 1% semiamplitude variation. Note that the amplitude of the measured light curve is not less than that of the input signal. [*See the electronic edition of the Journal for a color version of this figure.*]

is not representative of noise expected for stars of this brightness, as extra noise is introduced in the sky-subtraction process. As is apparent from Figure 2, the light curves are in good agreement with the simulated signal.

4. PHOTOMETRIC PRECISION

In Figure 3 we plot the rms of each light curve versus the average magnitude for that light curve. We plot each night separately for both the entire mosaic and the best individual chip (labeled 21 in Fig. 1).

For reference we also plot the 6.5 σ detection limits for Jupiter- and Neptune-sized transiting planets. These lines are defined by equation (3) in Mochejska et al. (2002):

$$\mathrm{rms} = \sqrt{N}\Delta R/\sigma, \tag{4}$$

where N is the number of observations in transit, ΔR is the amplitude of the transit, and σ is set to 6.5. To calculate N we use the length of a transit as given by equation (1) of Gilliland et al. (2000):

$$\tau = 1.412 M_*^{-1/3} R_* P^{1/3}, \tag{5}$$

where τ and P are in days, and the stellar mass, M_*, and radius, R_*, are in solar units. To obtain M_* and R_* as functions of magnitude we generated isochrones from Girardi et al. (2000) using the parameters for the cluster listed in § 2. The lines were then calculated for a $P = 3.5$ day period planet assuming one observes three full transits with 2 minute integrations taken every 3 minutes for comparison with night 2, and 1 minute integrations taken every 2 minutes for comparison with night 3. The implications of these lines are discussed in § 6.

There are a total of 378 stars that have rms < 1 mmag on the second night, and 9661 with rms < 10 mmag. For the third night, with the shorter exposure times, we find 365 stars with rms < 1 mmag and 8132 with rms < 10 mmag. When the two nights are combined we find only 65 stars with rms < 1 mmag and 7732 with rms < 10 mmag. The drastic reduction in the number of stars with rms < 1 mmag is not unexpected, as the differing exposure times between the two data sets results in a different saturation level. To estimate what fraction of these stars are likely to be cluster members we constructed the surface density profile consisting of all stars with rms < 1 mmag and all stars with rms < 10 mmag. From this we estimate that the field surface density of stars with rms < 1 mmag is $\sim$0.2 arcmin^{-2} on the second night and $\sim$0.5 arcmin^{-2} on the third night, and for those with rms < 10 mmag it is $\sim$10 arcmin^{-2} on both nights. Thus, we estimate that $\sim$280 of the stars on the second night and $\sim$130 of the stars on the third night with rms < 1 mmag are cluster members, while for stars with rms < 10 mmag, $\sim$5000 and $\sim$3400 are cluster members.

From Figure 3 it is clear that the observed rms values are consistent with photon statistics for all but the brightest magnitudes. For stars brighter than $R = 16$ mag there appears to be an additional source of error contributing to the rms. To determine this constant error for each chip on the second and third nights we estimated the rms in magnitudes of the jth light curve as

$$\sigma_j = \sqrt{\sum_{i=1}^{n} \frac{[2.5 \log_{10}(e)]^2 (F_{ji} + s_i)}{g_{\mathrm{eff}} n F_{ji}^2} + c^2}, \tag{6}$$

where n is the number of images, $F_{ji} = 10^{2(z_i - m_{ji})/5}$ is the flux in ADU of the jth light curve on the ith image, z_i is the zero point of the ith image, m_{ji} is the magnitude of the jth light curve on the ith image, s_i is the effective sky flux of the ith image, g_{eff} is the effective gain of the chip, and c is the constant error term for the chip. When performing PSF fitting the above equation is applicable except that the effective gain is less than the actual gain, with the exact factor depending on the shape of the PSF and the size of the region one uses to fit the PSF (see eq. [37] of Kjeldsen

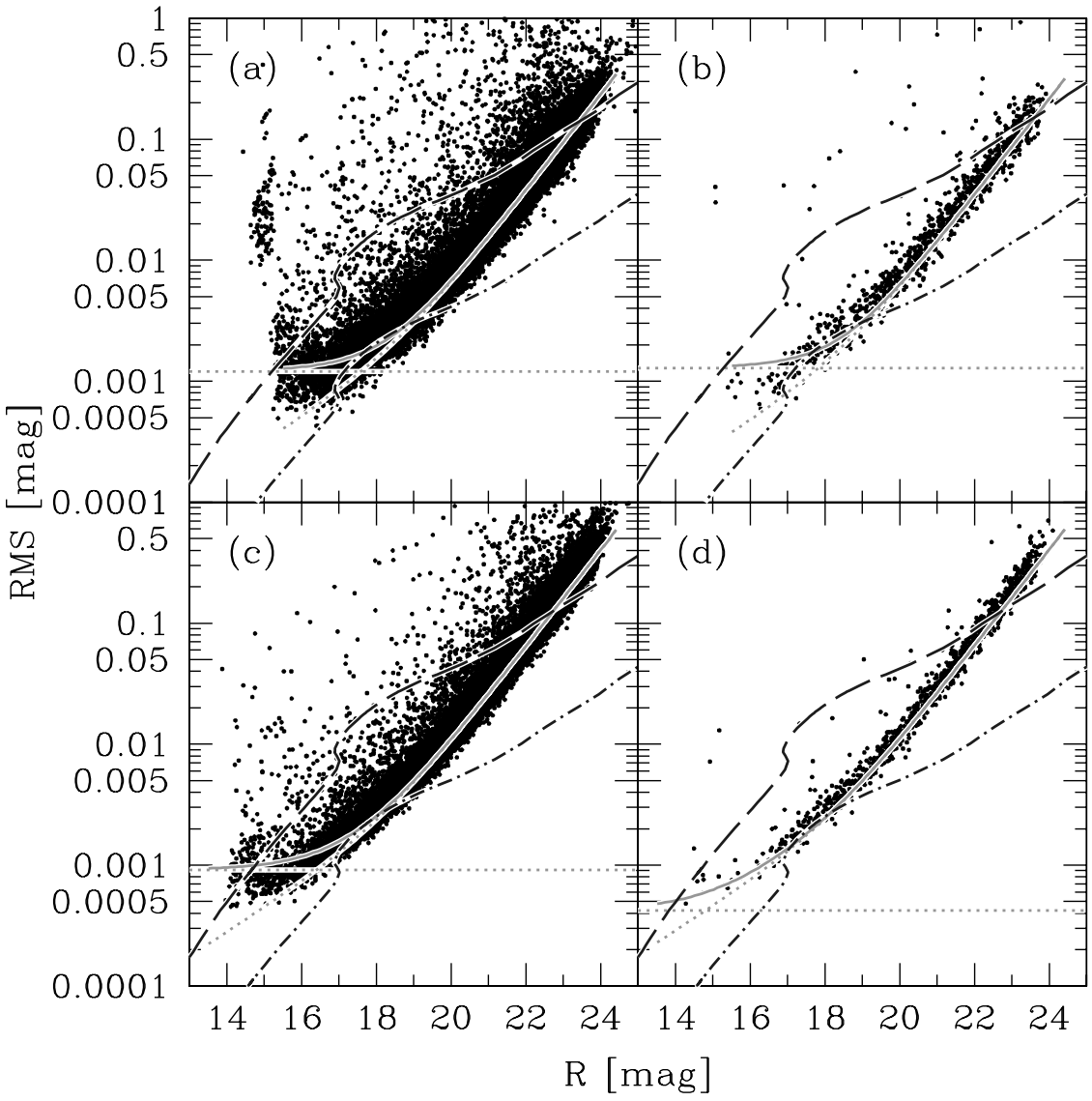

FIG. 3.—Light curve rms vs. magnitude plotted for (*a*) chips 1–33 on night 2, (*b*) chip 21 on night 2, (*c*) chips 1–33 on night 3, and (*d*) chip 21 on night 3. The solid line shows a fit to the observed errors including photon noise and a constant error term (*dotted lines*); the dashed line shows the 6.5 σ detection limit for a transiting Jupiter-sized planet, while the dot-dashed line shows the same limit for a transiting Neptune-sized planet. The generation of these lines is described in § 4, and we discuss the implications in § 6. [*See the electronic edition of the Journal for a color version of this figure.*]

& Frandsen [1992] for the case of a Gaussian PSF). We find values for the effective gain that are typically less than the actual gain of the CCD by a factor of $\sim$1.7.

We find that on the second night the constant error term ranges from 0.56 to 2.4 mmag with an average value (over stars) of 1.2 mmag, while for the third night the constant error term ranges from 0.42 to 1.6 mmag with an average value of just below 1 mmag. We also note that stars faint enough for the errors to be dominated by photon statistics have a lower rms in the second night compared to the third by a factor that is consistent with the longer exposure time for the second night.

When the data for the second and third nights are combined, the rms on some chips is not increased for stars that are well below saturation in both nights ($R < 16.5$). However, there are chips for which there appears to be greater scatter in the rms of the bright stars. When using the TMZ05 algorithm this scatter is reduced for all the chips so that the rms versus magnitude plot for the two combined nights is comparable to that of the rms versus magnitude plot for an individual night (see Fig. 4). This implies that any systematic variations between nights can be corrected for using the TMZ05 algorithm.

There are a number of possible sources for the observed constant error term in our photometry. The relative error in the photometry (in magnitudes) due to Poisson noise in the flat field is (Kjeldsen & Frandsen 1992)

$$c_{\rm ff} = \frac{2.5 \log_{10}(e)}{N_{\rm ff}^{1/2}}, \tag{7}$$

where $N_{\rm ff} = \Omega_{\rm eff} e_{\rm ff}$, $\Omega_{\rm eff}$ is the effective area of the PSF in pixels, and $e_{\rm ff}$ is the total number of electrons in the flat field in one pixel. For the third night the combined flat field has $e_{\rm ff} = 3.3 \times 10^5$ electrons for each 2×2 pixel, and the FWHM ranged from 6 to 12 2×2 pixels. Thus, the expected constant error term due to flat-fielding lies below 0.2 mmag, well below the measured constant error terms for that night. This calculation assumes that the flat-fielding error is dominated by shot noise, the actual error may be larger if there are other systematic errors in

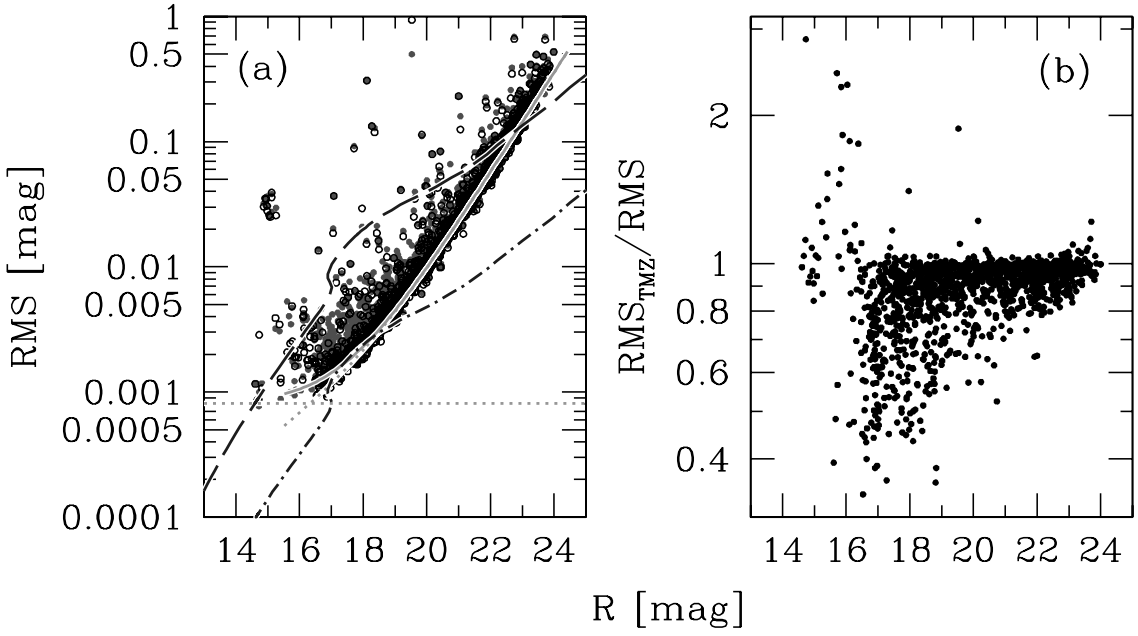

FIG. 4.—(*a*) Comparison between the precision of the light curves combined from the second and third nights when using the TMZ05 cleaning algorithm (*open circles*) and when not using it (*filled circles*). The lines shown are analogous to those in Fig. 3. (*b*) Ratio of the rms of the light curves cleaned and not cleaned with the TMZ05 algorithm. The TMZ05 algorithm appears to reduce the overall scatter in the rms at the bright end and can lower the rms of an individual light curve by as much as a factor of 3. The data in both plots is from a single chip (labeled 14 in Fig. 1). [*See the electronic edition of the Journal for a color version of this figure*.]

the flat field. The effect of this error is reduced when the pointing is stable between images. We note that because the PSF is so well sampled on the Megacam CCDs we do not expect intrapixel variations in the quantum efficiency to make a significant contribution to the error.

Atmospheric scintillation also adds an effective constant error term to the photometry. This error can be estimated from Young (1967) as

$$c_{\rm scint} = 0.1 d^{-2/3} X^{1.75} \exp(-h/8000)(2t_{\rm exp})^{-1/2}, \qquad (8)$$

where we use $c_{\rm scint}$ for the constant error term due to scintillation, d is the telescope diameter in centimeters, X is the air mass, h is the observatory altitude in meters, and $t_{\rm exp}$ is the exposure time in seconds. The leading coefficient is rather approximate [we multiply by $2.5 \log_{10}(e)$ to convert to magnitudes], as scintillation can change by a factor of 2 in a few minutes (e.g., Young 1993). For the second night, our observations were 60 s long, with the air mass ranging from 1.12 to 1.37. The MMT is located at an altitude of 2606 m and has a diameter of 650 cm. Therefore, we expect a constant error term of less than about 0.15 mmag due to atmospheric scintillation, and thus the total constant error term should be less than 0.25 mmag.

Because one obtains the PSF only once on the reference, the error in the PSF will not contribute to the errors in differential photometry. Instead, errors in the kernel that is used to convolve the PSF effectively add a constant error term to the photometry. It is difficult to estimate a priori exactly what that error should be, and we suspect that the constant error term that we have measured is due to this effect. To test this hypothesis we have also performed simple unit-weight aperture photometry on the subtracted images, the results for a single chip on the third night are shown in Figure 5. To correctly scale the fluxes we divided by the integral of the PSF over the aperture radius. We varied the aperture radius to optimize the precision at the bright end while providing correct amplitudes for the simulated variable stars mentioned in § 3. The aperture photometry light curves were then put through the cleaning procedures described in § 3 to provide a fair comparison with the optimal PSF light curves. As expected, unit-weight aperture photometry performs worse than PSF fitting for faint stars, as it is subject to a greater degree of sky background; however, for the brightest stars aperture photometry

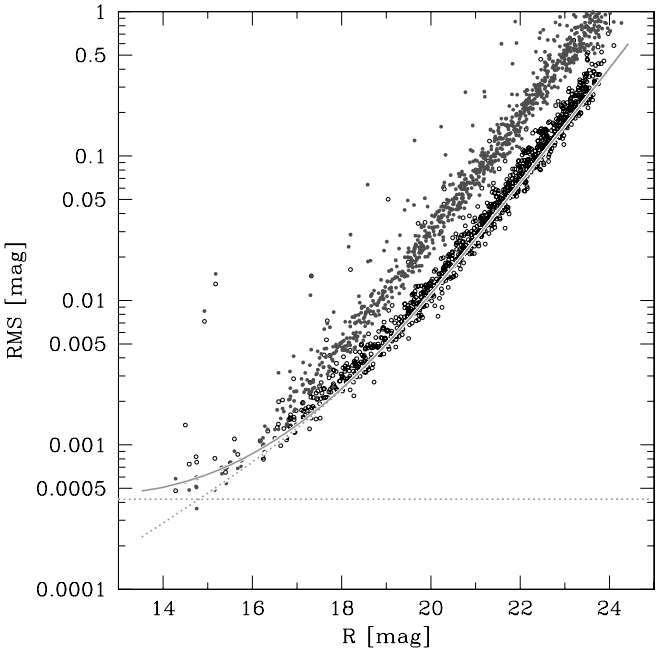

FIG. 5.—Comparison between the precision from performing aperture photometry on the subtracted images (*filled circles*) and PSF photometry on the subtracted images (*open circles*) for chip 21. The curves are the same as those in Fig. 3*c*. Note that aperture photometry appears to provide better precision for the brightest stars, while it provides worse photometry for fainter stars as the result of an effectively higher sky flux through the unweighted aperture. [*See the electronic edition of the Journal for a color version of this figure*.]

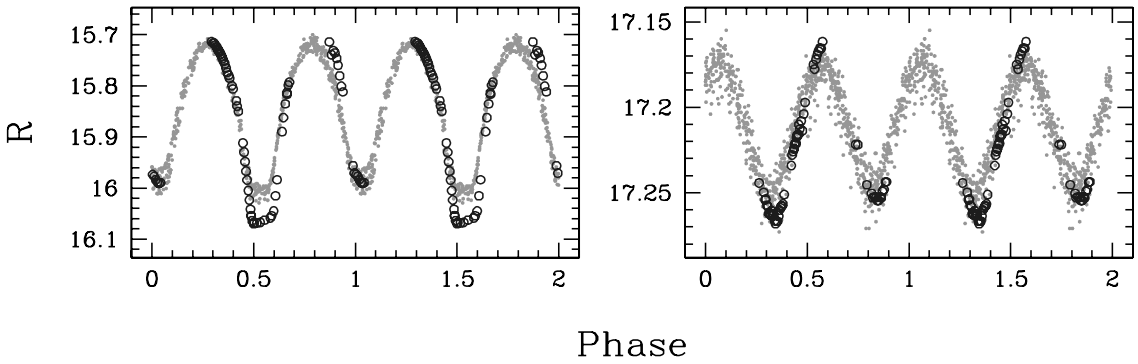

FIG. 6.—Comparison between our light curves (*open circles*) and those from PISCES (*filled circles*) for two known variable stars: V1 (*left*) and V4 (*right*). An arbitrary constant has been added to our light curves to provide alignment with the PISCES light curves. [*See the electronic edition of the Journal for a color version of this figure*.]

outperforms PSF fitting and appears to show no evidence of a constant error term. This effect is well known when not using image subtraction and confirms our suspicions that the constant error term arises from uncertainties in the kernel propagated through PSF fitting. Using aperture photometry on the subtracted images we achieve a precision as good as 0.36 mmag per exposure.

5. VARIABLE STARS

As a check on our photometry we compare our light curves for two known variables with those published by Mochejska et al. (2005) in Figure 6. It is clear from the light curves that our photometry matches well.

While the short time coverage of our observations prevents us from performing a systematic survey for variable stars, we have identified 10 new variables in the field of NGC 6791 and seven suspected variables that show evidence for low-amplitude, short-period variability. Table 1 lists the coordinates and basic photometric data for these variables, which we identify as V115–V124 and SV1–SV7. These stars were selected for their short-period variability using the Schwarzenberg-Czerny algorithm (Schwarzenberg-Czerny 1996) as implemented in a code due to Devor (2005). We checked the images of these stars to ensure that they were not located near bad columns or strongly saturated stars.

We present phased light curves for the newly discovered variables in Figure 7 and for the suspected variables in Figure 8.[4] For some of the suspected variable stars we have omitted the data from the first night when the noise is greater than the amplitude of variability in the second two nights. Due to a lack of time coverage the periods are tentative.

From the light curves we classify V115, V117, V118, and V120–V124 as likely W UMa–type contact binary systems. The variable V116 has a period and light curve shape that is typical of a δ Scuti–type pulsating star. Lacking color information for this star, we cannot verify whether this identification is correct. We note that differences between the variations on the three days show possible evidence for multiple modes of pulsation. Also note the precision of this 20 mmag amplitude light curve, particularly for the second and third nights. The light curve of V119 is similar to that of an RS CVn–type spotted star. All these variables lie outside of the field studied by PISCES, which is why they were not detected by that project.

The suspected variables (SV1–SV7) show very small full-amplitude variations, as low as 4 mmag in the case of SV2. The periods of these variables are also very short, between 2 and 11 minutes. Of these candidates, SV2–SV6 all lie within the field studied by PISCES; however, the periods are shorter than the PISCES exposure times. If real, the detection of these subtle variations represents an exciting demonstration of the potential of MMT and Megacam for precision time-series campaigns.

In cleaning our light curves we implemented the TMZ05 algorithm, which improved the light-curve rms when the second and third nights of data were combined. It is important to check whether or not this algorithm removes actual variability as well as systematic trends in the data. As a check on this possibility we compare the light curves of some of our new variables before and after using TMZ05 (Fig. 9). It is clear that the TMZ05 algorithm does not appreciably reduce the variability of any of our identified variable star candidates. In Figure 9 we also show two examples of light curves for which the TMZ05 algorithm does appear to reduce the amplitude of a variable signal. Both of these stars were initially identified as suspected variable candidates;

TABLE 1
NEW VARIABLE STARS IDENTIFIED IN THE FIELD OF NGC 6791

ID	$\alpha_{2000.0}$	$\delta_{2000.0}$	Period (days)	R (mag)	A_R (mag)
V115.....	19 19 50.29	37 58 32.9	0.367505	19.96	0.286
V116.....	19 20 10.22	37 43 12.2	0.049967	16.21	0.020
V117.....	19 20 36.36	37 39 56.7	0.393266	17.27	0.363
V118.....	19 20 51.00	37 39 03.9	0.258878	17.35	0.526
V119.....	19 21 07.07	37 54 58.9	0.113333	17.48	0.137
V120.....	19 21 10.54	37 40 22.3	0.268731	19.82	0.165
V121.....	19 21 29.03	37 55 56.3	0.267418	16.92	0.598
V122.....	19 21 38.63	37 38 29.4	0.185982	20.58	0.523
V123.....	19 21 43.46	37 39 56.9	0.107470	16.79	0.123
V124.....	19 21 54.52	37 40 53.4	0.527230	17.31	0.510
SV1	19 20 49.26	37 45 11.6	0.002042	17.87	0.005
SV2	19 20 50.29	37 40 06.7	0.007476	16.83	0.004
SV3	19 20 50.99	37 43 59.2	0.003531	17.45	0.006
SV4	19 21 06.06	37 44 43.7	0.002188	20.11	0.049
SV5	19 21 07.13	37 48 39.5	0.002190	19.04	0.018
SV6	19 21 15.50	37 49 56.1	0.002913	18.32	0.011
SV7	19 21 53.42	37 49 44.9	0.004522	16.82	0.005

NOTES.—The first 10 entries are confirmed variables, while the last seven are low-amplitude suspected variables. Coordinates are from 2MASS where available. Units of right ascension are hours, minutes, and seconds, and units of declination are degrees, arcminutes, and arcseconds. The periods listed are those used to phase the light curves in Figs. 7 and 8 and should not be treated as constrained values for the periods. Amplitudes are defined as the difference between the second-brightest and second-faintest observations in the data presented in Fig. 7, while average magnitudes are flux-weighted.

[4] Light curves for all objects are available on request.

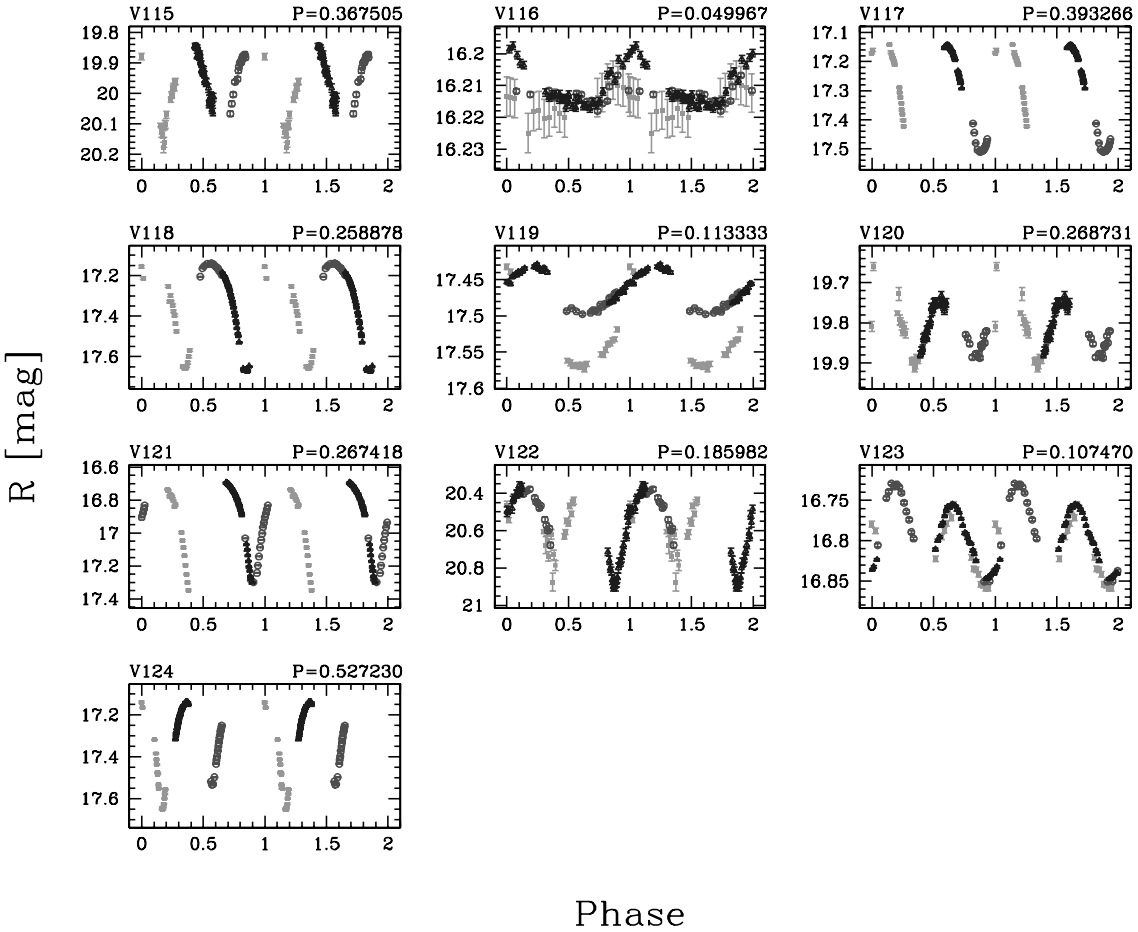

FIG. 7.—Phased light curves for newly discovered variables. Data from the first night are shown as filled squares, the second night as open circles, and the third night as open triangles. The expression P is the period in days. [*See the electronic edition of the Journal for a color version of this figure.*]

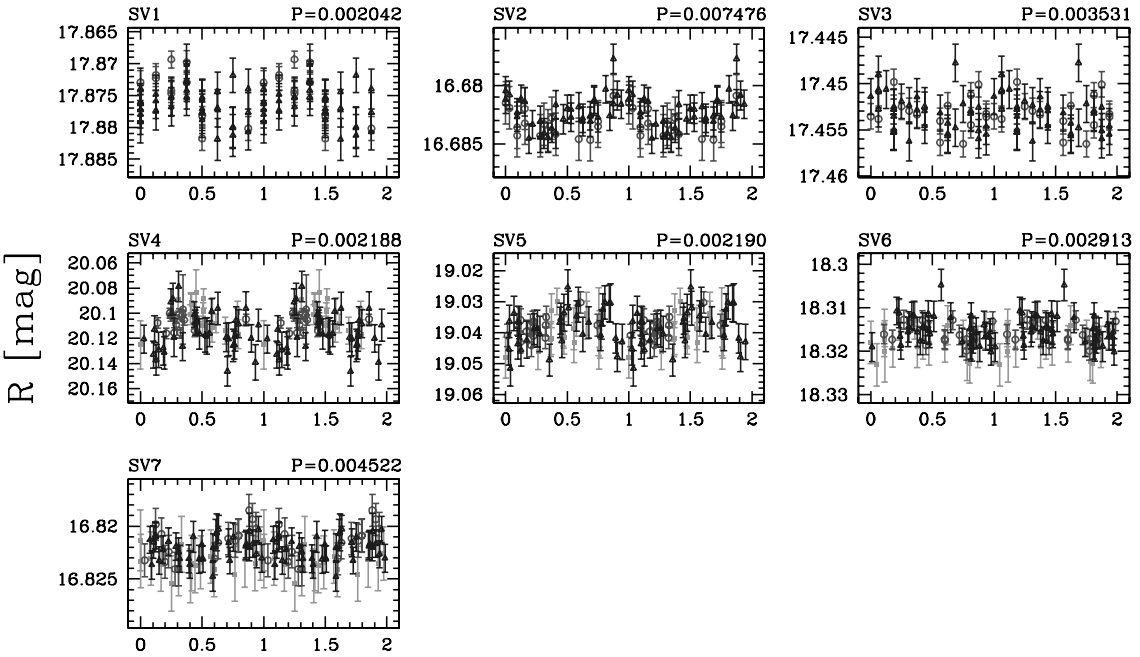

FIG. 8.—Same as Fig. 7, this time showing light curves of the suspected variable stars. We do not show data from the first night for the suspected variables when the noise from that night is greater than the amplitude of variability from the last two nights. [*See the electronic edition of the Journal for a color version of this figure.*]

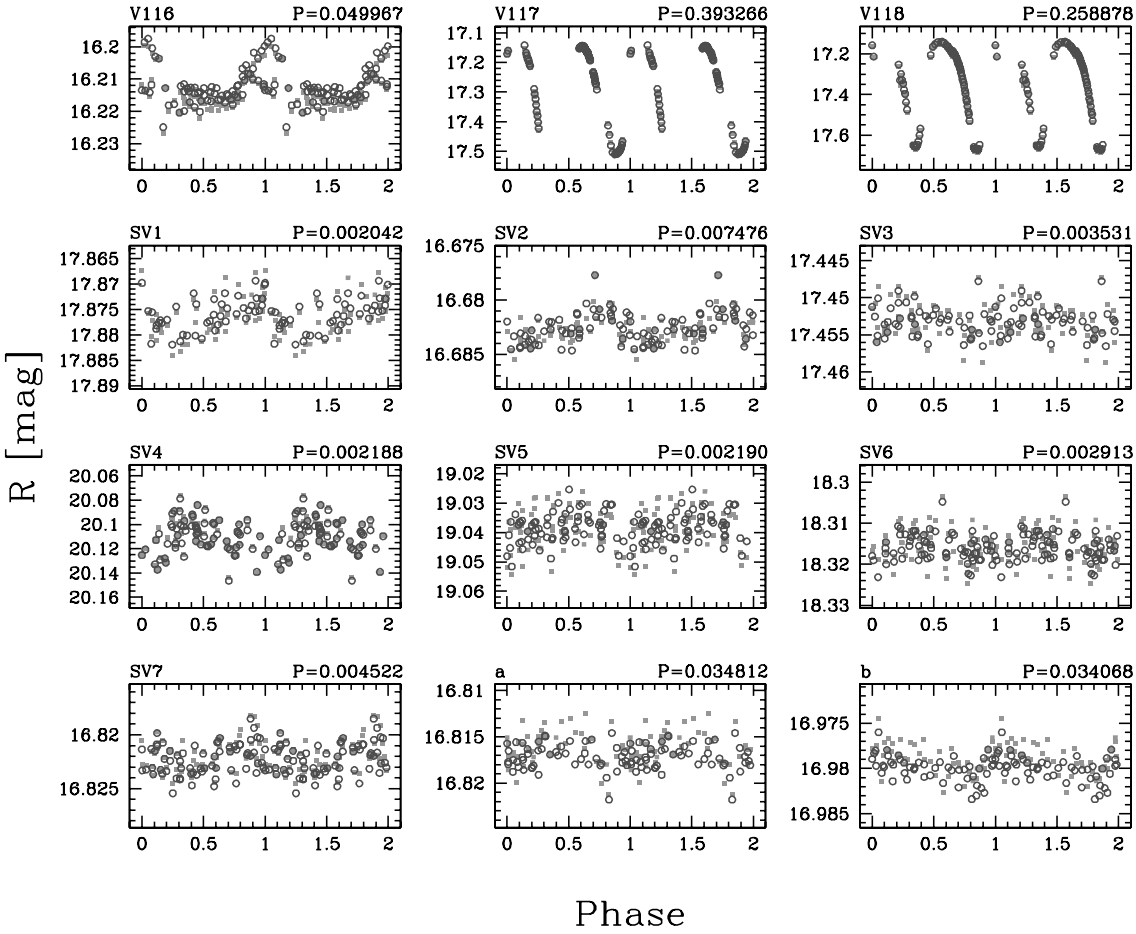

FIG. 9.—Comparison of the light curves from before and after using the TMZ05 trend-removing algorithm for a few new variable stars and all of the suspected variable stars. The light curves before using TMZ05 are shown as filled squares, and the light curves after using TMZ05 are shown as open circles. We also plot two light curves (labeled *a* and *b*) for stars whose variability appeared to be reduced by the TMZ05 algorithm. Note that none of the new variable stars or suspected variables appear to show substantial differences after using TMZ05. [*See the electronic edition of the Journal for a color version of this figure.*]

however, because TMZ05 appears to single out their variations as potential trends, we reject these light curves as candidates.

6. DISCUSSION

We have successfully demonstrated the capability of the MMT and Megacam to achieve very high precision photometry, as low as 0.360 mmag at the bright end, for a large number of stars. In the process we have discovered 10 new variable stars and have identified seven possible variable stars with amplitudes as low as 4 mmag. While we have not broken the record so to speak for the best precision per exposure obtained from the ground, we have achieved submillimagnitude photometry from the ground for more stars at once than has ever been reported. Our results with aperture photometry on the subtracted images shows that there are no barriers to our ability to achieve precisions of a few hundred micromagnitudes with this telescope and instrument. The fact that we did not require modified hardware or a significantly new observing technique to achieve this level of precision suggests that other observers interested in conducting large-scale, photometric, time-series surveys could reasonably attempt to achieve submillimagnitude precision.

While the detection of solar-like, *p*-mode oscillations in other stars is difficult to do in a reasonable amount of time, even with submillimagnitude photometry (see, e.g., Gilliland et al. 1993), we can still probe a relatively unexplored regime of stellar variability.

Another exciting application of this technology could be to survey stellar clusters for planets as small as Neptune. In Figures 3–5 we showed the 6.5 σ detection limits for planets as small as Neptune assuming one observed three full transits with MMT and Megacam. For the second night, with the 2 minute exposure time, there are 23,062 stars below the Jupiter detection limit, assuming they are all cluster members, and 1664 stars below the Neptune detection limit. On the third night, with the 1 minute exposures, there are 19,843 stars below the Jupiter detection limit and 648 stars below the Neptune detection limit. From the surface density profile of these stars we can estimate the field surface density and hence estimate that for the second night there are $\sim$9000 cluster members below the Jupiter detection limit, and $\sim$1000 cluster members below the Neptune detection limit. For the third night the numbers are $\sim$8000 and $\sim$400, respectively.

The ability to detect Jupiters in this system is not limited by precision but rather the time baseline over which observations are carried out. If one observes long enough to have a reasonable chance of detecting 2–3 full transits, then one would be able to find essentially every short-period, transiting, Jupiter-sized planet in the stellar cluster. Since there are only three known planets with a lower mass limit near that of Neptune (Santos et al. 2004b; McArthur et al. 2004; Butler et al. 2004), essentially nothing is known about the statistics of Neptune-sized planets. Moreover, because all these planets have been detected only via their influence on the radial velocities of their host stars, we do not know anything about their radii. Therefore, the very fact that there are hundreds of stars around which we could detect transiting,

Neptune-sized planets if they exist represents an exciting new opportunity for the study of extrasolar planets.

As noted by Pepper & Gaudi (2005), as a result of the relations between mass, luminosity, and radius for main-sequence stars, if one can identify a transiting planet around any cluster member with source-limited precision, then one could find that same transiting planet around essentially all cluster members with source-limited precision. The effect of this is that it is not essential for planet finding to achieve source-limited photometry at the brightest end where there are few stars, rather it is most important to achieve source-limited photometry for a large number of stars. Therefore, even if our photometry shows some small (<1 mmag) constant error term at the bright end, we would still have sensitivity to Neptune-sized planets around many stars. Thus, it is not fundamentally the ability to do high-precision photometry just below saturation that opens up the possibility of finding small planets, but rather it is the fact that we are using a large telescope that can collect a greater signal per exposure for every star compared with using a smaller telescope.

We can estimate the number of planets one could detect in an ambitious, many-night survey of NGC 6791 using Megacam on the MMT. Adopting the parameters of NGC 6791 listed previously [$E(B-V) = 0.1$, distance $= 4.8$ kpc, age $= 8$ Gyr] and assuming a mass function slope and normalization that reproduces the empirical I-band luminosity function of Kaluzny & Udalski (1992), we calculate the number of planets one would detect as a function of the planetary radius using the formalism of Pepper & Gaudi (2005). We assume that the planets are uniformly distributed in log period, and we consider planets with periods $P = 1-3$ and $3-9$ days separately. For our fiducial calculation, we assume a detection threshold of S/N > 6.5, 7 hr per night, 0.1% systematic error, and perfect weather. We then consider the effect of changing each of these fiducial assumptions on the number of detected planets. Figure 10 shows the number of detected planets as a function of radius, under the assumption that every star has a planet of a given radius. As mentioned above, NGC 6791 has a supersolar metallicity of [Fe/H] $= 0.3-0.4$ dex, which implies a frequency of hot Jupiters ($P = 3-9$ days) of $\sim$4% (Fischer & Valenti 2005; Santos et al. 2004a; Mochejska et al. 2005) and a frequency of very hot Jupiters ($P = 1-3$ days) of $\sim$0.6% (Gaudi et al. 2005), assuming the population of planets is similar to the local solar neighborhood. For our fiducial assumptions, these frequencies yield $\sim$5 expected detections of hot Jupiters and $\sim$3 expected detections of very hot Jupiters.

One is unlikely to detect a significant number of hot Neptunes in NGC 6791, unless they are considerably more common than their massive counterparts. However, NGC 6791 is not necessarily ideal for the detection of hot Neptunes, and closer clusters will likely yield improved expected detection rates. To demonstrate this, in Figure 10 we also show the number of expected

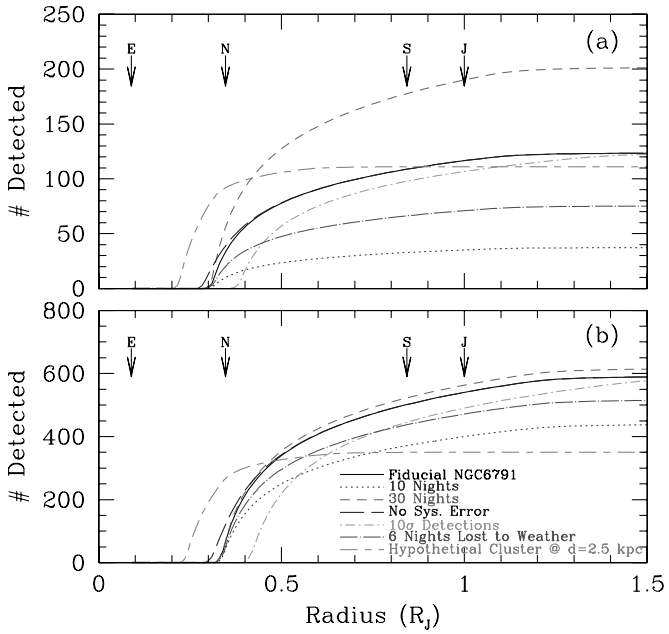

FIG. 10.—Expected number of (*a*) hot planets ($P = 3-9$ days) and (*b*) very hot planets ($P = 1-3$ days) detected as a function of planetary radius assuming that all stars have planets of the given radius within the stated periods. For the fiducial calculation we assume 20 nights of perfect weather, 7 hr per night, and a detection threshold of 6.5 σ. [*See the electronic edition of the Journal for a color version of this figure.*]

detections for a hypothetical cluster with the same parameters as NGC 6791 but with a distance of 2.5 kpc, 2500 stars, 10 hr per night, and 0.5% systematic error. In this case, one would expect to detect $\sim 90f$ hot Neptunes and $\sim 270f$ very hot Neptunes, assuming that a fraction f of stars have Neptune-sized planets in the given range of periods. Finally, we mention that the weather in Arizona also makes NGC 6791 a nonoptimal target for the MMT. At 19^h21^m of right ascension, the cluster is best observed in July/August and is thus subject to the Arizona monsoon season. We have also obtained preliminary data for the open clusters M35 and NGC 2158. The results from these clusters will be presented in a future contribution.

We gratefully acknowledge B. Mochejska for the use of data from PISCES in calibrating our photometry and for helpful discussions. We also acknowledge G. Pojmanski for his excellent "lc" program and W. Pych for his "fwhm" program. J. D. H. is funded by a National Science Foundation Graduate Student Research Fellowship. K. Z. S. acknowledges support from the William F. Milton Fund. B. S. G. is supported by a Menzel Fellowship from the Harvard College Observatory.

REFERENCES

Alard, C. 2000, A&AS, 144, 363
Alard, C., & Lupton, R. H. 1998, ApJ, 503, 325
Alonso, R., et al. 2004, ApJ, 613, L153
Bouchy, F., Pont, F., Santos, N. C., Melo, C., Mayor, M., Queloz, D., & Udry, S. 2004, A&A, 421, L13
Bruntt, H., Grundahl, F., Tingley, B., Frandsen, S., Stetson, P. B., & Thomson, B. 2003, A&A, 410, 323
Butler, P., et al. 2004, ApJ, 617, 580
Chaboyer, B., Green, E. M., & Liebert, J. 1999, AJ, 117, 1360
Devor, J. 2005, ApJ, 628, 411
Everett, M. E., & Howell, S. B. 2001, PASP, 113, 1428
Fischer, D. A., & Valenti, J. 2005, ApJ, 622, 1102
Gaudi, B. S., Seager, S., & Mallen-Ornelas, G. 2005, ApJ, 623, 472
Gilliland, R. L., & Brown, T. M. 1992, PASP, 104, 582
Gilliland, R. L., et al. 1993, AJ, 106, 2441
———. 2000, ApJ, 545, L47
Girardi, L., Bressan, A., Bertelli, G., & Chiosi, C. 2000, A&AS, 141, 371
Hartman, J. D., Bakos, G., Stanek, K. Z., & Noyes, R. W. 2004, AJ, 128, 1761
Horne, K. 2003, in ASP Conf. Ser. 294, Scientific Frontiers in Research on Extrasolar Planets, ed. D. Deming & S. Seager (San Francisco: ASP), 361
Jha, S., Charbonneau, D., Garnavich, P. M., Sullivan, D. J., Sullivan, T., Brown, T. M., & Tonry, J. L. 2000, ApJ, 540, L45
Kaluzny, J., & Ruciński, S. M. 1993, MNRAS, 265, 34
Kaluzny, J., & Udalski, A. 1992, Acta Astron., 42, 29

Kjeldsen, H., & Frandsen, S. 1992, PASP, 104, 413
Konacki, M., Torres, G., Jha, S., & Sasselov, D. D. 2003, Nature, 421, 507
Konacki, M., Torres, G., Sasselov, D. D., & Jha, S. 2005, ApJ, 624, 372
Konacki, M., et al. 2004, ApJ, 609, L37
Kurtz, D. W., et al. 2005, MNRAS, 358, 651
McArthur, B., et al. 2004, ApJ, 614, L81
McLeod, B. A., Conroy, M., Gauron, T. M., Geary, J. C., & Ordway, M. P. 2000, in Proc. International Conference on Scientific Optical Imaging, Further Developments in Scientific Optical Imaging, ed. M. Bonner Denton (Cambridge: Royal Soc. Chemistry), 11
Mochejska, B. J., Stanek, K. Z., & Kaluzny, J. 2003, AJ, 125, 3175
Mochejska, B. J., Stanek, K. Z., Sasselov, D. D., & Szentgyorgyi, A. H. 2002, AJ, 123, 3460
Mochejska, B. J., et al. 2005, AJ, 129, 2856
Pepper, J., & Gaudi, B. S. 2005, ApJ, 631, 581
Pont, F., Bouchy, F., Queloz, D., Santos, N. C., Melo, C., Mayor, M., & Udry, S. 2004, A&A, 426, L15
Pont, F., Melo, C. H. F., Bouchy, F., Udry, S., Queloz, D., Mayor, M., & Santos, N. C. 2005, A&A, 433, L21
Press, W. H., Teukolsky, S. A., Vettering, W. A., & Flannery, B. P. 1992, Numerical Recipes in C: The Art of Scientific Computing (2nd ed.; New York: Cambridge Univ. Press)
Ruciński, S. M., Kaluzny, J., & Hilditch, R. W. 1996, MNRAS, 282, 705
Santos, N. C., Israelian, G., & Mayor, M. 2004a, A&A, 415, 1153
Santos, N. C., et al. 2004b, A&A, 426, L19
Schwarzenberg-Czerny, A. 1996, ApJ, 460, L107
Stetson, P. B. 1987, PASP, 99, 191
———. 1992, JRASC, 86, 71
Tamuz, O., Mazeh, T., & Zucker, S. 2005, MNRAS, 356, 1466 (TMZ05)
Tonry, J. L., Howell, S. B., Everett, M. E., Rodney, S. A., Willman, M., & VanOutryve, C. 2005, PASP, 117, 281
Udalski, A., Pietrzynski, G., Szymanski, M., Kubiak, M., Zebrun, K., Soszynski, I., Szewczyk, O., & Wyrzykowski, L. 2003, Acta Astron., 53, 133
Udalski, A., Szewczyk, O., Zebrun, K., Pietrzynski, G., Szymanski, M., Kubiak, M., Soszynski, I., & Wyrzykowski, L. 2002a, Acta Astron., 52, 317
Udalski, A., Zebrun, K., Szymanski, M., Kubiak, M., Soszynski, I., Szewczyk, O., Wyrzykowski, L., & Pietrzynski, G. 2002b, Acta Astron., 52, 115
Udalski, A., et al. 2002c, Acta Astron., 52, 1
Young, A. T. 1967, AJ, 72, 747
———. 1993, Observatory, 113, 41